

Aerodynamic Analysis of a Spinning Missile with Dithering Canards

Tor A. Nygaard*

Eloret Corporation, Sunnyvale, California 94087

and

Robert L. Meakin†

NASA Ames Research Center, Moffett Field, California 94035

A generic spinning missile with dithering canards is used to demonstrate the utility of an overset structured grid approach for simulating the aerodynamics of rolling airframe missile systems. A grid convergence study and assessment of viscous effects shows that a medium-resolution viscous grid with 8 million grid points provides a good compromise between solution accuracy and throughput. Viscous effects should be included in detailed studies to capture the interaction between the inboard canard vortex and the fuselage and tail boundary layers. The computed results agree well with experimental data. A database of cases with variation of angle of attack and the strength of control authority of a pitch-up maneuver is computed to evaluate missile performance. The case throughput rates are sufficient to contemplate population of aerodynamic databases with Navier–Stokes computations. Overall, the structured overset grid approach enables accurate and efficient simulation of rolling airframe missile configurations that involve relative motion between system components.

Nomenclature

A	=	reference area, where $A/L^2 = 0.0020$
C_{mx}	=	rolling moment coefficient, $M_x / \frac{1}{2} \rho_\infty U_\infty^2 A L_{\text{ref}}$
C_{my}, C_{mz}	=	pitching and yawing moment coefficients
C_p	=	pressure coefficient, $(p - p_\infty) / \frac{1}{2} \rho_\infty U_\infty^2$
C_x	=	axial force coefficient, $F_x / \frac{1}{2} \rho_\infty U_\infty^2 A$
C_y, C_z	=	side and normal force coefficients
c	=	command level
F_x, F_y, F_z	=	axial, side, and normal forces
L	=	missile length nose to base
L_{ref}	=	reference length, where $L_{\text{ref}}/L = 0.0505$
M	=	Mach number
M_x, M_y, M_z	=	rolling, pitching, and yawing moments
p	=	pressure
Re	=	Reynolds number based on L
U	=	air speed
y^+	=	turbulent wall coordinate
α	=	angle of attack
ρ	=	air density
Ω_D	=	dither frequency
Ω_R	=	roll rate

Subscript

∞	=	freestream
----------	---	------------

Introduction

DIRECTIONAL control of nonspinning missiles is commonly achieved by using four canards. If the missile spins, two canards are sufficient to obtain control in both pitch and yaw. This

could result in a simpler system from a mechanical point of view. Experimental and computational evaluations of missile performance, however, become more complicated because we now have an unsteady problem. Simulation of the unsteady aerodynamics of rolling airframe missile systems pose significant challenges for any computational approach. Applications of practical interest are characterized by complex vortical flow and shock structures. In addition, the geometry of these missile systems can be very complex, involving relative motion between missile fuselage and control surfaces. The aim of this paper is to demonstrate the utility of Chimera¹ overset structured grid domain decomposition methods in the efficient generation of high-fidelity aerodynamic simulations for this class of problems. This study was part of a larger effort to compare several computational approaches on selected rolling airframe systems. Nygaard and Meakin² used an overset approach to perform Reynolds averaged Navier–Stokes (RANS) computations. Hall³ used an overset approach to perform laminar Navier–Stokes computations. Murman et al.⁴ used a multi level Cartesian method to perform Euler computations. Blades and Marcum⁵ used an unstructured grid approach⁶ to perform RANS computations. We are not aware of any earlier computational fluid dynamics (CFD) applications involving dynamic computations of spinning missiles with control surfaces moving relative to the fuselage.

A generic rolling airframe missile is defined to demonstrate the advantages and limitations of an overset grid approach. The paper provides a technical description of the generic missile and the specific computational methods here employed, as well as discussions of the case conditions and corresponding simulation results. The set of simulations considered is designed to demonstrate the level of resolution required for accurate prediction of surface loads and to determine the aerodynamic significance of viscous effects. Computations are compared with experimental data. The aerodynamic performance of the missile as a function of angle of attack and canard pitching sequence is also considered.

Rolling Airframe Configuration

The generic rolling airframe missile employed in the present work is referred to as FM-3. The coordinate system is defined as follows: origin, missile nose; x axis, nose to tail; y axis, side; and z axis, up. The FM-3 missile has a hemispherical nose, cylindrical body, four fins, and two canards. Details of the geometric complexity of the missile are shown in Fig. 1. The fins are designed to induce missile spin, whereas directional control is actuated via canard dithering.

Received 23 September 2002; revision received 9 July 2003; accepted for publication 15 July 2003. Copyright © 2003 by the American Institute of Aeronautics and Astronautics, Inc. The U.S. Government has a royalty-free license to exercise all rights under the copyright claimed herein for Governmental purposes. All other rights are reserved by the copyright owner. Copies of this paper may be made for personal or internal use, on condition that the copier pay the \$10.00 per-copy fee to the Copyright Clearance Center, Inc., 222 Rosewood Drive, Danvers, MA 01923; include the code 0022-4650/04 \$10.00 in correspondence with the CCC.

*Research Scientist, 690 West Fremont Avenue. Member AIAA.

†Senior Staff Scientist, U.S. Army Aroflightdynamics Directorate, Aviation and Missile Command, Army/NASA Rotorcraft Division. Senior Member AIAA.

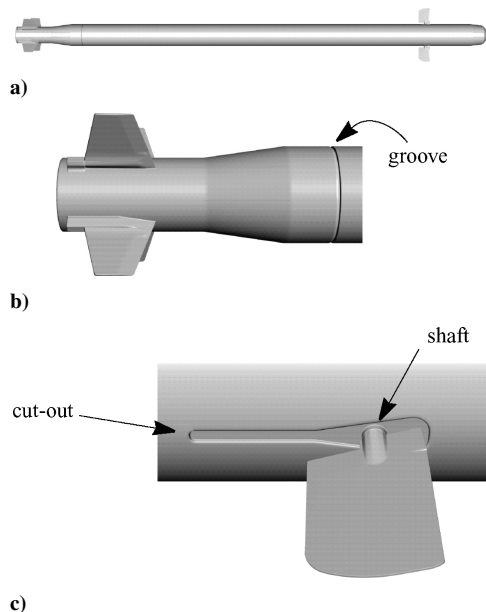


Fig. 1 FM-3 missile geometry.

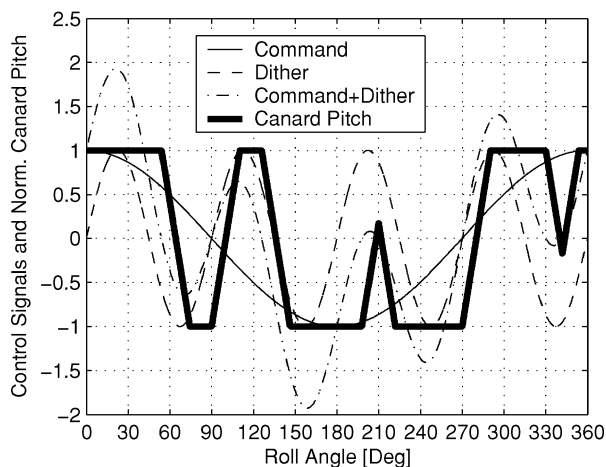


Fig. 2 Canard pitching algorithm.

The present study uses three analytical pitching sequences that are periodic over one revolution. As the missile spins, the canard pitch position chases an actuator signal with constant pitch rate. The actuator signal flip-flops between ± 1 according to the sign of the sum of two sine waves called the command and dither signals. The amplitude of the command signal relative to the amplitude of the dither signal is called the command level and reflects the strength of the attempted maneuver. The command signal is modulated with the roll rate. The dither signal is modulated with the dither frequency. The phase angle of the command signal is related to the direction the missile is attempting to maneuver. The phase angle is zero for all cases considered in the present work. Figure 2 shows the canard pitching algorithm for a command level of 100%, for a dither frequency four times the roll rate. Figure 3 shows the three analytical pitching sequences used in the present study. The 0% command level is symmetric. For zero angle of attack, the roll-averaged effect of this pitching sequence is zero both in pitch and yaw. A positive command level with zero phase angle results in mainly a nose-up pitching moment and a small yawing moment.

Model Description

The near-body and off-body domain partitioning method⁷ is used here as the basis of discretization of the FM-3 missile. In the approach, the near-body portion of a domain is defined to include the surface geometry of all bodies being considered and the volume of space extending a short distance away from the respective surfaces.

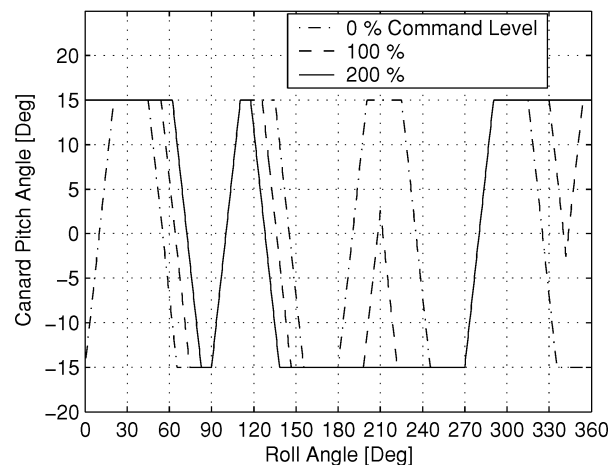


Fig. 3 Canard pitching sequences.

The construction of near-body grids and associated intergrid connectivity is a classical chimera-style decomposition of the near-body domain. It is assumed that near-body grids provide grid point distributions of sufficient density to resolve accurately the flow physics of interest, that is, boundary layers, vortices, etc., without the need for refinement. This is a reasonable constraint because near-body grids are only required to extend a short distance away from body surfaces.

The off-body portion of the domain is defined to encompass the near-body domain and extend out to the far-field boundaries of the problem. The off-body domain is filled with overlapping uniform Cartesian grids of variable levels of refinement. The grid spacing doubles for each successive level of off-body grids. The near-body off-body partitioning approach facilitates grid adaptation in response to proximity of body components and/or to estimates of solution error within the topologically simple off-body grid system.

The set of FM-3 missile simulations presented in this paper are products of the OVERFLOW-D⁸ code. OVERFLOW-D is based on version 1.6au of the well-known NASA OVERFLOW⁹ code but has been significantly enhanced to accommodate moving-body applications. The OVERFLOW-D enhancements represent in-core subroutine actuated operations and include the following capabilities: 1) on-the-fly generation of off-body grid systems, 2) message passing interface (MPI) enabled scalable parallel computing, 3) automatic load balancing, 4) aerodynamic force and moment computations, 5) general six-degree-of-freedom model, 6) rigid-body relative motion between an arbitrary number of bodies, 7) domain connectivity, 8) solution error estimation, and 9) grid adaptation in response to body motion and/or estimates of solution error.

In cases that involve relative motion between configuration components, body dynamics and domain connectivity are addressed at each time step. Because the missile movement is continuous, the relative positions of many grid components change at every time step. For solution information to be correctly exchanged between grids during the simulation, the domain connectivity solution must also be continuously updated. This is accomplished automatically by OVERFLOW-D. The OVERFLOW-D processing rate for static geometry viscous flow applications is about $15 \mu\text{s}$ per grid point per time step (300-MHz processor). For moving-body problems, the processing rate is somewhat problem dependent, but generally falls in the bounds of $15\text{--}18 \mu\text{s}$ per grid point per time step.

OVERFLOW-D accommodates problem sizes of more than 2 million grid points per 1 GB of memory. Maximum parallel efficiency (percentage in high nineties) is realized when the fewest number of processors that can accommodate a given problem in core memory are selected. OVERFLOW-D can efficiently, that is, over 70%, make use of larger numbers of processors for a fixed problem size when each processor assumes the load of at least 250,000 points. Load balancing is an automatic function of OVERFLOW-D. OVERFLOW-D accommodates solution adaptation based on the position of near-body grid components and/or in response to estimates of solution error. The off-body grid management scheme allocates

level-1 (finest) resolution grids to accommodate significant motion of body components or flow features before the next adapt cycle. Accordingly, adapt cycles are only required periodically, every 25 to 50 time steps in a typical unsteady simulation.

In the FM-3 missile cases considered here, all flow features that are likely to have any significant effect on the surface forces and moments are confined to the volume of space within a missile diameter of the body itself. These include canard vortices, boundary layers, and key portions of the shock systems. Accordingly, OVERFLOW-D input is used to allocate level-1 resolution capacity to a distance of 1.5 diameters from the missile surface, rather than enable adaptation in response to solution error. A slight savings in computational overhead is thereby gained for the present cases. The flow solver configuration used for the Navier–Stokes computations in the present work is the following: 1) central differences, second order in space; 2) ARC3D three-factor diagonal implicit time-stepping scheme, first order in time; 3) second- and fourth-order filtering for both left- and right-hand side; 4) Baldwin–Barth one-equation turbulence model; 5) time step for the time-accurate computations: sound wave travels 0.25% of the missile length per time step; 6) the extent of the domain is -3.0 to 5.0 in the x direction and -4.0 to 4.0 in both the y and z directions; and 7) inflow/outflow subsonic/supersonic conditions based on the characteristics used on the boundaries of the domain. [Note that coordinates for the nose and tail of the missile in this Cartesian system are $(0, 0, 0)$ and $(1, 0, 0)$ respectively.]

Simulation Results

Resolution Requirements

A grid refinement study is used to determine the level of spatial resolution needed to predict accurately the integrated FM-3 surface loads. The significance of grid resolution is evaluated here by comparing viscous solutions for the spinning missile case defined in Table 1 with the variable parameters c , α , and Ω_R fixed at 0%, 3 deg, and 8.75 Hz, respectively.

A high-resolution grid is used to define the baseline solution. Medium and coarse solutions are obtained on grids derived from the baseline grid with successively lower levels of spatial resolution. The baseline grid for this case (finest resolution) comprise 41 million grid points and is referred to hereafter as the viscous-1 (V1) grid. Isolated surfaces from the V1 grid are shown in Figs. 4 and 5. All grid lengths referred to in the following discussion are normalized by the missile body length. Viscous spacing normal to the body surfaces is 2.5×10^{-6} in the V1 grid. This corresponds to a y^+ of 1 for a Reynolds number of 10×10^6 . This spacing is maintained uniformly across the first 6 cells in the viscous direction and then expanded with a geometric stretching ratio of 1.2 to a distance of approximately 0.015. The maximum spacing used in the near-body grids is approximately equal to the level-1 off-body grid spacing equal to 0.0013.

The V1 grid is the basis of the medium (V2) and coarse (V3) grids. The V2 grid is obtained by deleting every other point from the V1 grid in all three spatial dimensions and results in a grid with just over 8 million points. Similarly, the V3 grid is obtained from the V2 grid by deleting every other point from the V2 grid in all three spatial dimensions and results in a grid with just over 2 million points. The foregoing is true subject to the following qualifications:

1) Some surface grids require redistribution and/or addition of grid points to preserve geometric features, such as sharp corners through the two subsequent eliminations of every other point.

Table 1 Baseline parameters

Parameter	Value
Mach number M_∞	1.6
Reynolds number Re	50×10^6
Dither frequency Ω_D	35 Hz
Angle of attack α	0, 2, 3, 4, 8, 12, and 15 deg
Command level c	0, 100, 200%
Roll rate Ω_R	0, 8.75 Hz

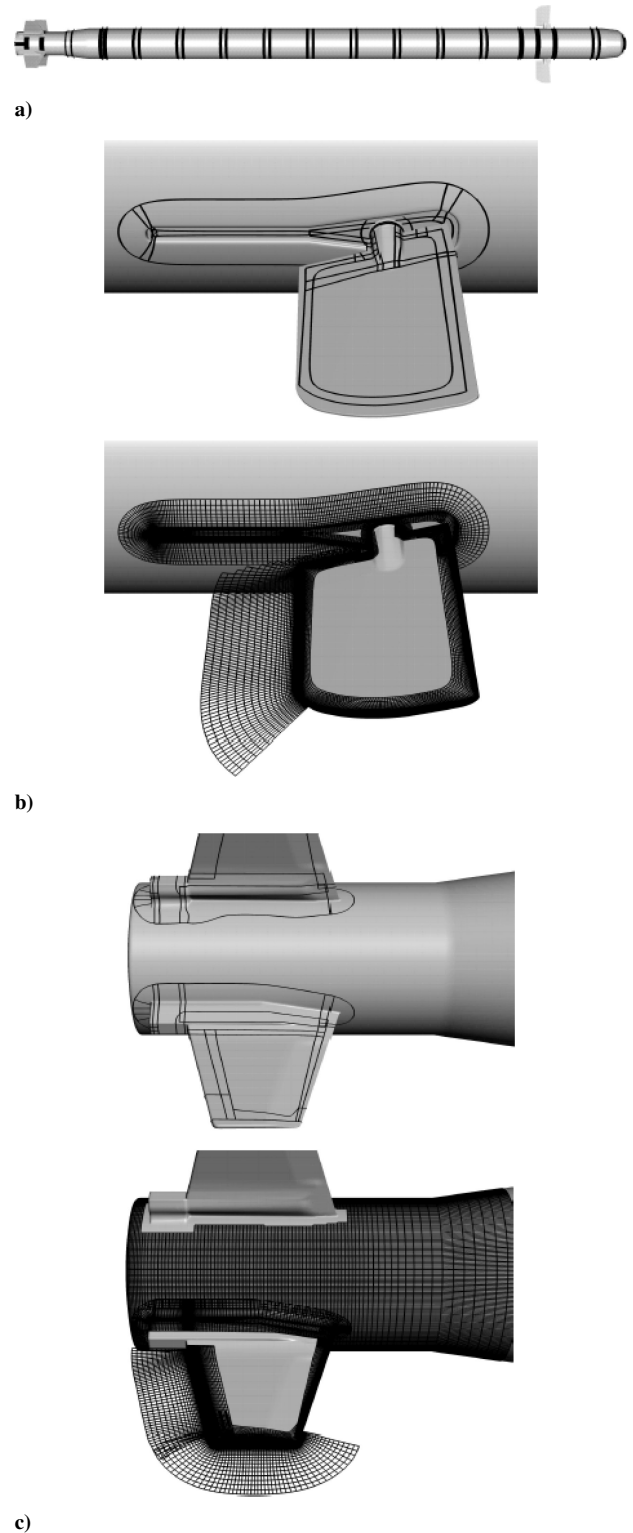


Fig. 4 FM-3 surface geometry definition and near-body grids.

2) Smoothing is applied to geometric features that are not adequately resolved by the coarser grids. For the V2 grid, smoothing is applied to the canard cutout and the missile groove. For the V3 grid, the canard cutout, the canard shaft, and the missile groove are removed completely.

3) The grid spacing in the surface normal direction for the V2 grid corresponds approximately to every other point for the V1 grid, doubling the initial spacing from the wall.

4) The grid spacing in the surface normal direction for the V3 grid starts at the surface with the V2 spacing doubled. The stretching ratio thereafter is approximately the same as in the V2 grid.

Table 2 Roll-averaged force and moment coefficients

Grid	Coefficient					
	C_x	C_y	C_z	C_{mx}	C_{my}	C_{mz}
Fine V1	1.17	-7.56×10^{-3}	0.461	-2.36×10^{-2}	-1.34×10^{-1}	5.54×10^{-2}
Medium V2	1.12	-2.76×10^{-3}	0.462	-2.14×10^{-2}	-6.16×10^{-2}	6.97×10^{-2}
Coarse V3	1.07	-1.21×10^{-3}	0.538	-1.86×10^{-2}	-0.683	-1.89×10^{-2}

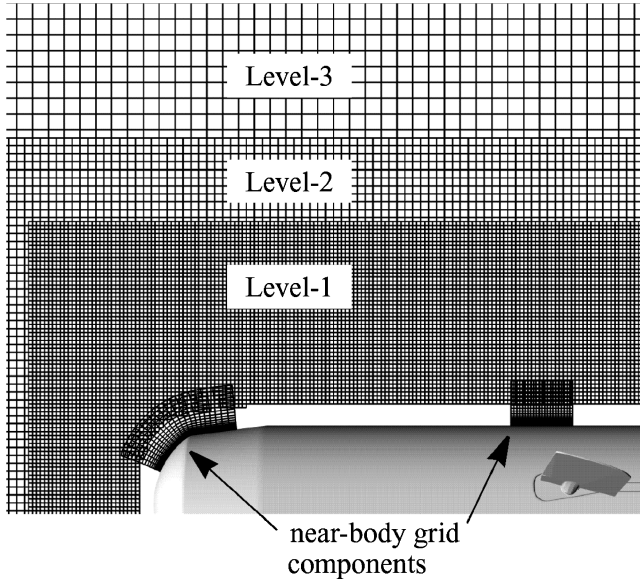


Fig. 5 FM-3 near-body and off-body partitioning and selected surfaces.

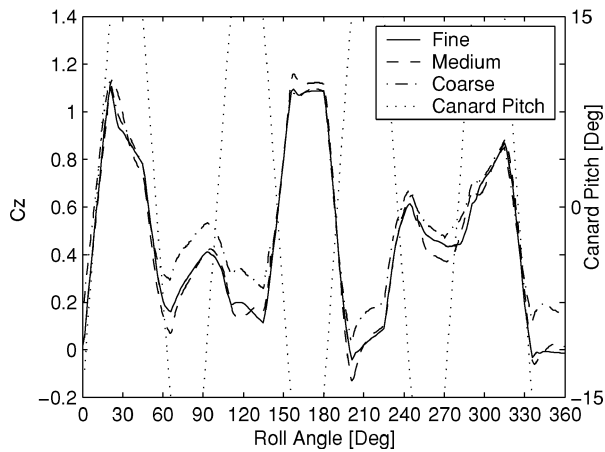


Fig. 6 Grid effects in the normal force coefficient.

Consider now the computed load histories obtained from simulations using the V1, V2, and V3 grids. All load histories presented in this paper are sampled after the solutions became periodic. Figure 6 shows the computed normal force C_z history for the three different resolution capacities. The canard pitch angle history is also indicated. The V1 and V2 results are in good agreement, except at maximum canard deflection. At high canard lift, the strong vortices shed from the canards modify the pressure distribution on the fuselage and the tail fins. Still, the roll-averaged normal forces from V1 and V2 shown in Table 2 differ by less than 0.3%, indicating grid convergence for this quantity. The V3 result differs significantly from V1 and V2. The side forces (only roll averages shown) exhibit the same effect as for the normal forces at maximum canard deflection. The roll-averaged side forces shown in Table 2 are close to zero, with a difference between V1 and V2 of less than 0.6% of the maxi-

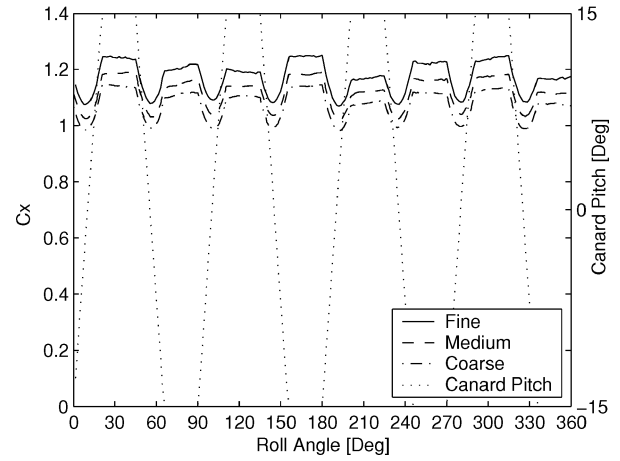


Fig. 7 Grid effects in the axial force coefficient.

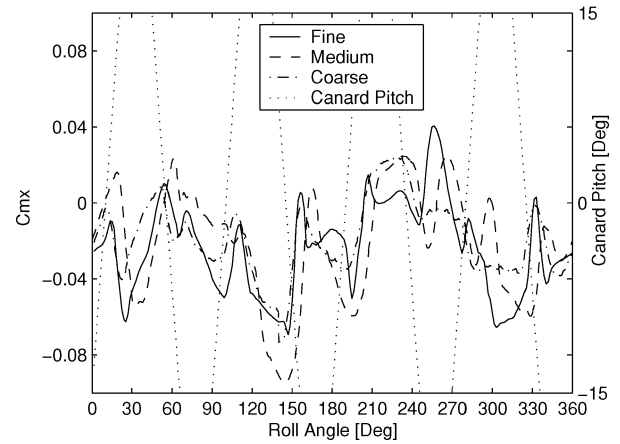


Fig. 8 Grid effects in the rolling moment coefficient.

um side force during a revolution, indicating grid convergence for this quantity also. The percentage of maximum side force is used here as a measure of grid convergence because the roll-averaged side force is small. The axial forces shown in Fig. 7, indicate a systematic shift to higher values for finer resolution. The roll-averaged axial forces are shown in Table 2. The medium and coarse solution axial forces are 4 and 8% lower than for the corresponding fine solution. The viscous and pressure forces contribute about equally to this difference. The pressure contribution is mainly from the aft part of the missile. This region of the flow has complicated interactions between the expansion waves around the boattail, shocks around the tail fins, and the boundary layer. The viscous contribution is a result of the coarser resolution in surface normal direction for the V2 and V3 grids.

The difference between the V1 and V2 roll-averaged pitching moments is approximately 1% of the maximum pitching moment during a revolution. The difference between the V1 and V2 roll-averaged yawing moments is approximately 0.2% of the maximum yawing moment during a revolution.

The rolling moment C_{mx} is shown in Fig. 8. As expected, the moments are small. A steady-state freely spinning missile should have

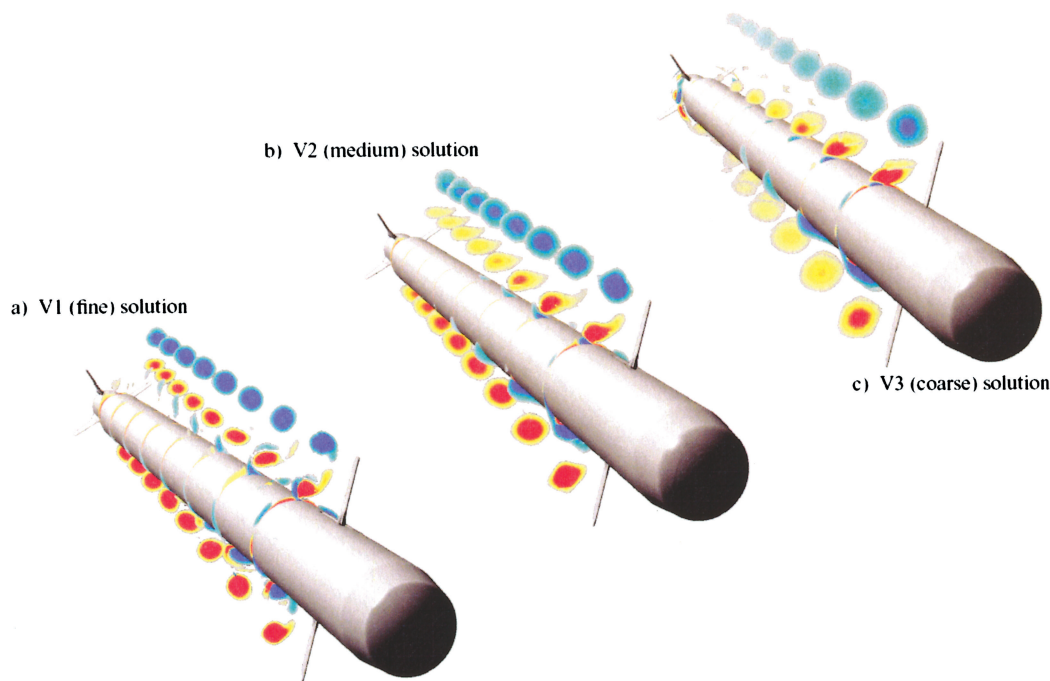


Fig. 9 Effect of grid resolution on canard vortices.

a roll-averaged rolling moment of zero. The overall pattern here is in fair agreement, but the details differ significantly. The rolling moment is sensitive to flow details around the tail fins, with complex interactions between the boundary layer, the canard vortices, and the shocks, which again depend on the accurate prediction of the flow along the entire missile. The difference between the V1 and V2 roll-averaged rolling moments is approximately 4% of the maximum rolling moment during a revolution. This is indicating a fair grid convergence for the overall rolling moment. The effect of grid resolution on the prediction of the aerodynamic details of the flow is shown in Fig. 9. The canard vortices and missile boundary-layer interactions are shown via plots of helicity density, that is, dot product of the velocity and vorticity vectors, at several stations along the length of the missile (for a roll-angle of 268.5 deg at maximum negative canard deflection). The position of the vortices are in good agreement for the V1 and V2 solutions. However, the vortex strength is weaker, and interactions between the inboard canard vortex and viscous boundary layer of the missile body are less apparent in the V2 solution. The V3 solution differs significantly from the V1 and V2 solutions in vortex position, strength, and vortex/boundary-layer interaction.

The grid refinement study shows good overall agreement between the V1 and V2 solutions. The V2 grid offers a good compromise between solution accuracy and solution throughput for computations designed to predict aerodynamic forces and moments.

Viscous Effects

A comparative evaluation of high-resolution Navier–Stokes and Euler simulations is used to determine the relative significance of viscous effects operative in the range of flight conditions considered for the FM-3 missile. The case conditions defined in Table 1 are taken as representative of these flight conditions.

The V1 solution considered is used as the basis of comparison for a correspondingly high-resolution inviscid simulation. The high resolution inviscid, or Euler grid, is referred to hereafter as the E1 grid system. The E1 surface grids and off-body volume grids are identical with the corresponding components of the V1 grid system. The only differences between the E1 and V1 grids is the surface normal distribution of points in the respective near-body grid components. The E1 surface normal wall spacing is 20 times that of the V1 grid. There are 33 million points used to define the complete E1 grid compared to the 41 million points used in V1.

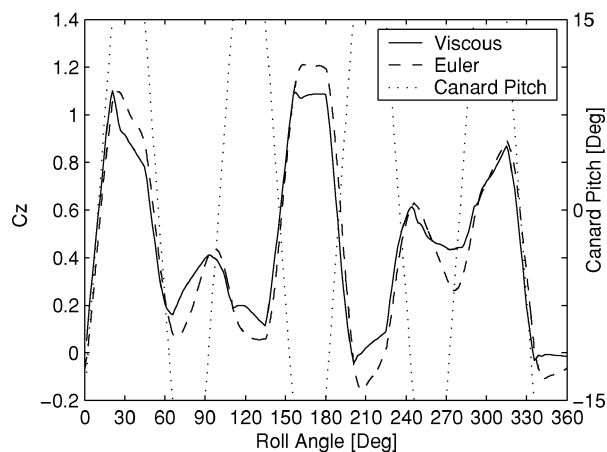


Fig. 10 Viscous effects in the normal force coefficient.

The computational savings available by assuming inviscid flow are significant. In the present high-resolution cases, 20% fewer grid points are used in the E1 system than in the V1 system. Because of the larger surface normal wall spacing, larger stable time steps are also possible, a Δt increase of 5 times is used in the present E1 simulations, resulting in approximately 2500 steps per missile revolution. In the present simulations, the combined effects of fewer grid points, fewer floating-point operations required per grid point, and larger time steps result in an order of magnitude savings in computational expense.

Consider viscous and inviscid solutions for the spinning FM-3 missile ($\Omega_R = 8.75$ Hz and $\Omega_D = 35$ Hz). The corresponding roll-averaged force and moment coefficients are given in Table 3.

Figure 10 shows the normal force histories over one revolution. The viscous and inviscid computations agree well, except at maximum canard deflection, where there are instantaneous differences of up to 20%. The influence of the deflected canards on overall forces appear more pronounced in the inviscid case, though this is an indirect effect. The differences are due to pressure differences on the fuselage and tail. The canard forces are almost identical for viscous and inviscid case. The vortex systems shed from the canards interact with the fuselage and tail fins differently in the viscous and inviscid solutions. The inviscid inboard canard vortices are too energetic and

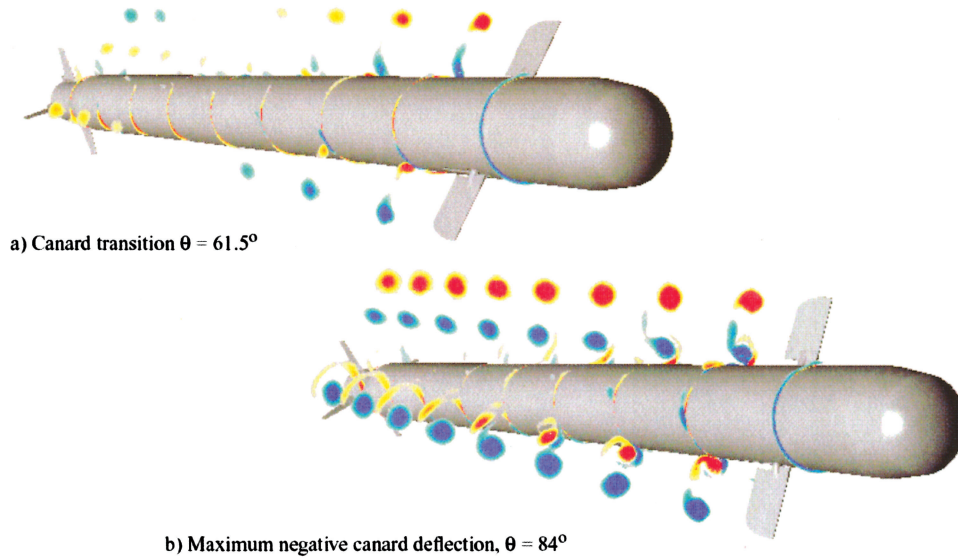
Table 3 Roll-averaged force and moment coefficients

Grid	Coefficient					
	C_x	C_y	C_z	C_{mx}	C_{my}	C_{mz}
Viscous V1	1.17	-7.56×10^{-3}	0.461	-2.36×10^{-2}	-1.34×10^{-1}	5.54×10^{-2}
Inviscid E1	1.10	-19.6×10^{-3}	0.449	-3.27×10^{-2}	-2.10×10^{-2}	1.82×10^{-1}

Table 4 Roll-averaged forces and moments, experimental pitching sequence

Method	Coefficient					
	C_x	C_y	C_z	C_{mx}	C_{my}	C_{mz}
Experiment	N/A	0.15–0.20	0.45–0.61	0.019–0.036	–1.5––0.40	–1.5––0.93
OVERFLOW-D	1.09	0.22	0.49	0.024	–0.85	–1.36
U ² NCLE ^a	1.12	0.22	0.51	0.023	–0.77	–1.5

^aUnstructured Unsteady Computation of Field Equations.


Fig. 11 Vortical structures for FM-3 spinning missile case.

positioned incorrectly. The same effects are true for the side forces. The reason that the viscous and inviscid solutions agree very well everywhere except at maximum canard deflection is evident in the vortical structures shown in Fig. 11. Figure 11a shows planes with helicity density contours at several stations along the length of the missile for a roll angle of 61.5° . At this roll angle, the canard is in transition between the maximum positive and negative canard pitch angles. Vortices trail each canard in counter-rotating pairs. Whenever the canards snap from positive to negative (or negative back to positive) pitch angle, the rotational sense of the vortices also reverse direction. From the canard downstream to about the missile midpoint, the vortices become weaker and finally disappear. From the midpoint back to the tail section, the vortices reappear rotating in the opposite sense and growing slightly in strength. The history of one transition cycle is captured in Fig. 11a. Vortex interaction with the boundary layer is minimal during canard transition. Accordingly, the viscous and inviscid solutions are in very good agreement for all roll angles where the canards are in transition.

Figure 11b shows cutting planes with helicity density contours at several stations along the length of the missile for a roll angle of 84° . The instantaneous solution indicated in Fig. 11b corresponds to the completion of nearly 20° of missile roll angle, or 2.5 missile body lengths of travel, with the canards positioned at maximum negative deflection. The fully developed canard vortices prevail well past the missile. The vortices interact with each other and with the boundary layer. The inboard canard vortices are weakened by the boundary layer, reducing the force peaks, as seen in the normal force histories of Fig. 10. The inboard canard vortex/boundary-layer interactions are entirely unaccounted for in an inviscid simulation.

The roll-averaged axial force for the viscous solution is about 8% higher than the corresponding inviscid solution (Table 3). Approximately 60% of the difference noted between the viscous and inviscid axial force is due to viscous wall stresses. The remaining 40% of the difference is due to spatial variations in the surface pressure distributions. Boundary-layer/shock interactions in the viscous solution lead to differences in overall shock structure and surface pressure distributions, accounting for these differences.

Based on the high resolution viscous (V1) and inviscid (E1) simulations, a few statements regarding the relative significance of viscous effects on FM-3 missile performance are justified:

1) Instantaneous side and normal forces differ up to 20%. This is due to differences in interaction between the vortex system shed from the canards and the fuselage boundary layer and tail fins.

2) The roll-averaged axial forces differ by about 8%. The viscous wall stresses accounts for 60% of this difference.

3) Euler computations provide valuable information for roll-averaged results. Viscous effects should be included in detailed studies.

Comparison with Experiments

The FM-3 missile has recently been tested in a wind-tunnel experiment.¹⁰ Results from the test include roll-averaged forces and moments, an analysis of uncertainty, and the measured canard pitch as function of roll angle. An analytic approximation to the ensemble average of canard pitch over 10 revolutions⁴ was used for computations with the V2 grid. The computed roll-averaged forces are shown in Table 4, along with experimental results and viscous CFD results from an unstructured grid flow solver.⁵

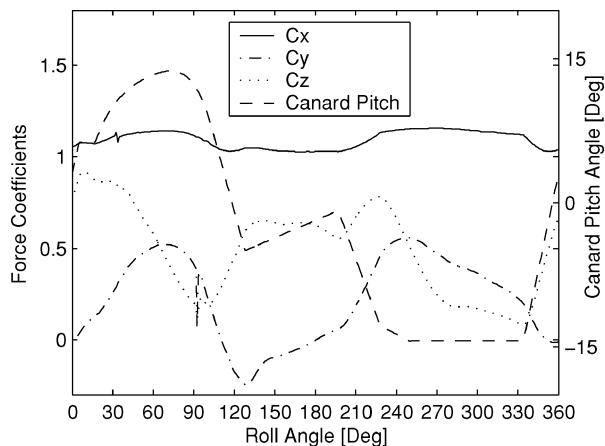


Fig. 12 Computed forces for experimental case.

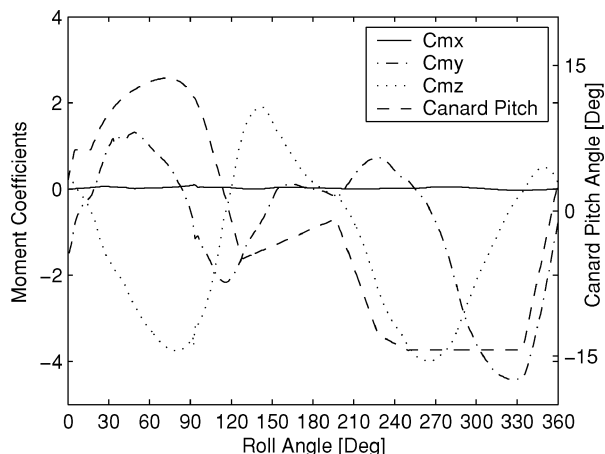


Fig. 13 Computed moments for experimental case.

The computed forces and moments over one revolution and the canard pitch sequence are shown in Figs. 12 and 13. The moment is taken at the initial center of gravity. The computed forces and moments are within the experimental uncertainty, except for the side force. The side forces are identical for the two CFD approaches and marginally outside the experimental interval. The difference between the computed side force and the upper limit of the experiment is less than 2% of the total force.

Overall, the grid convergence study and comparison with experimental results indicate that the current modeling approach is useful for computing forces and moments on the FM-3 missile.

Aerodynamic Performance

A matrix of cases is defined to evaluate the aerodynamic performance of the FM-3 spinning missile subject to variations in freestream angle of attack α and canard command level c . The baseline conditions for the case matrix are defined by the fixed parameters of Table 1 (Mach number M_∞ , Reynolds number Re , and Ω_D) and with the roll rate Ω_R set to 8.75 Hz. The matrix consists of 21 unique cases defined by varying α and c over the ranges indicated in Table 1. The viscous effects study demonstrate that although inviscid computations can provide valuable information about the FM-3 spinning missile, there are significant viscous effects, for example, fuselage boundary-layer damping of the inboard canard vortex. The results also indicate that the medium resolution viscous grid (V2) yields comparable results to the 41 million point baseline viscous grid (V1). Accordingly, the case matrix considered here is populated entirely with viscous solutions using the V2 grid system. The cost of generating 21 time-accurate spinning missile solutions to populate the case matrix is far less expensive than generating a comparable database composed of quasi-static solutions. Time-accurate simulation data are, therefore, used. The normal forces for the seven cases

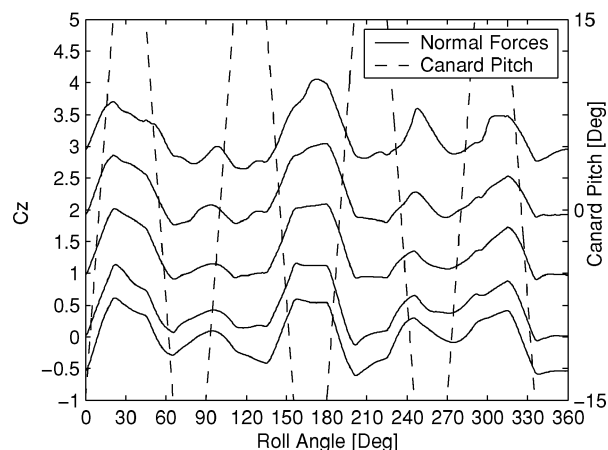


Fig. 14 Normal force coefficients for $\alpha = 0, 3, 8, 12$, and 15 deg at 0% command level.

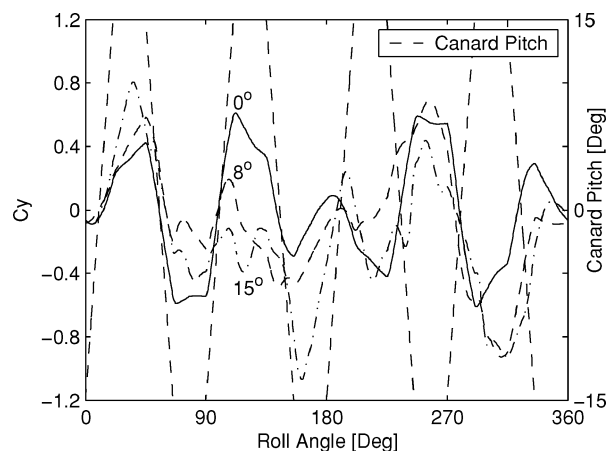


Fig. 15 Side force coefficients for different α at 0% command level.

with command level 0% are shown in Fig. 14. Results for the 2- and 4-deg angle of attack fall smoothly between neighboring data points and are omitted in Fig. 14 for clarity. The effect of increased α is a shift of the normal force curves upward, with a limited change in variation with roll angle. This is true also for the cases with 100 and 200% command level. The variation of the normal forces with roll angle is mainly caused by the normal force variations on the canards, as a direct result of the canard motion.

The side forces for three selected cases at 0% command level are shown in Fig. 15. The effect of α here is less clear than for the normal force. An increase of α increases the variation of side force. An interesting result apparent in Fig. 15 is nonzero side forces at roll angles of 0 and 180 deg (canards horizontal). This is due to the induced circulation from the missile spin interacting with the vertical component of the upstream velocity vector. This is similar to the Magnus effect on a spinning golf ball.

The roll-averaged normal forces are shown in Fig. 16. The normal force response to command level is nonlinear. The increment of normal force for the 200% command is not twice the increment for the 100% command level. Increasing the command level beyond 200% adds only limited control authority.

The roll-averaged side forces are shown in Fig. 17. The side forces increase slightly with command level. Further more, at each command level, the side force goes from positive to negative with increasing angle of attack. The negative side force at high α is caused partly by the Magnus effect, as mentioned earlier. The roll-averaged pitching moments about the center of gravity are shown in Fig. 18. The increase in pitching moment with command level is consistent with the increase in normal force for the canard. A change in command level to maneuver the missile affects the pitching moment in a similar manner for different α . The roll-averaged yawing moments

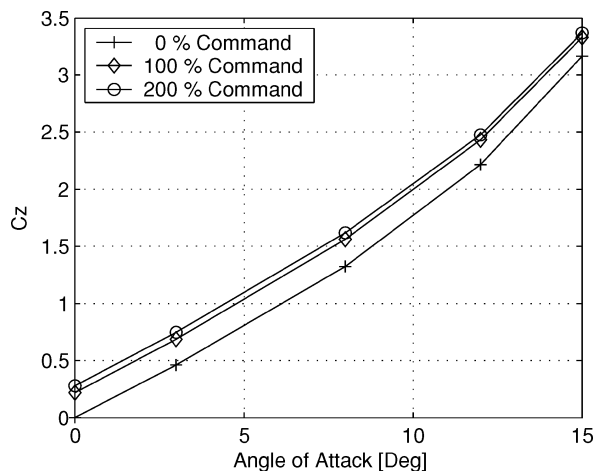


Fig. 16 Roll-averaged normal force coefficients for the case matrix.

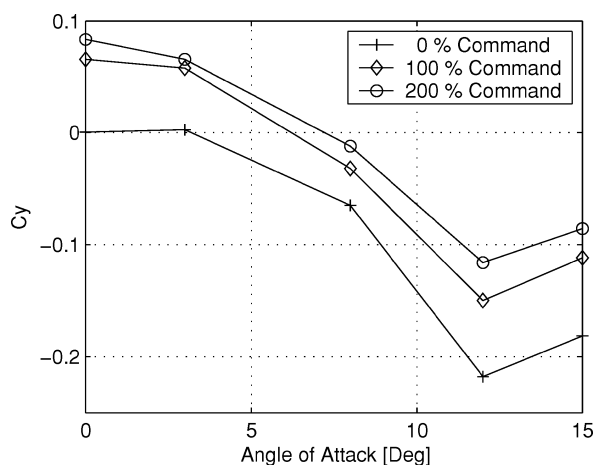


Fig. 17 Roll-averaged side force coefficients for the case matrix.

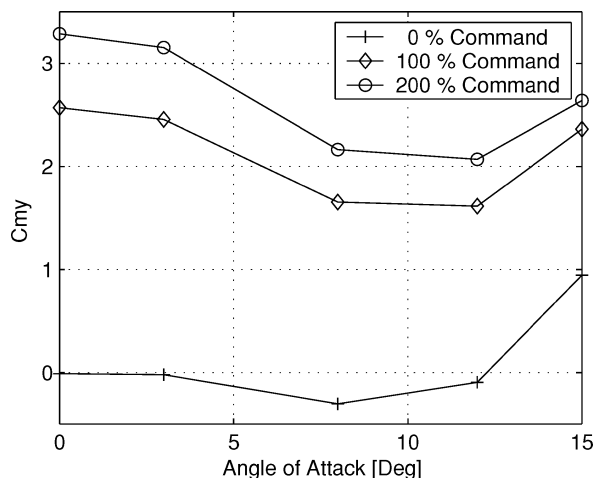


Fig. 18 Roll-averaged pitching moment coefficients for the case matrix.

about the center of gravity are shown in Fig. 19. The negative contribution from an increase of command level is consistent with the increase in canard side force.

Computational Expense

The FM-3 missile cases converge to a periodically repeating solution in approximately 460 deg of roll. The computational expense of each V2 time-accurate solution is approximately 438 h of CPU time on a 300-MHz processor, namely, SGI Origin 2000, per revolution, or 560 CPU hours per case. Most of the V2 results presented in this

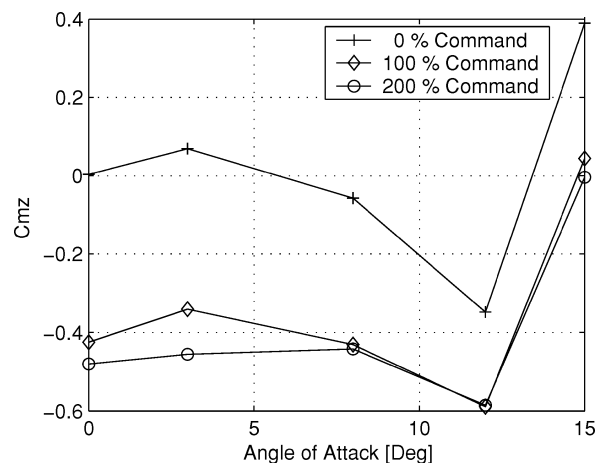


Fig. 19 Roll-averaged yawing moment coefficients for the case matrix.

paper are the result of runs using 16 processors, with a processing rate of 35 h per case and approximately 95% parallel efficiency.

The OVERFLOW-D performance rate realized for the V2 solutions justifies the contemplation of aerodynamic database population with Navier-Stokes solutions. Maximum parallel efficiency per case is realized when the minimum number of processors that will accommodate the case in core memory is used. Four processors are sufficient for the V2 solutions (assuming 1 GB of memory per processor). Simultaneous computation of multiple cases leads to perfect parallelism in the generation of solution sets. For example, a 256 node SGI Origin 2000 can execute 64 FM-3 cases simultaneously, yielding a throughput of approximately 330 cases per month. A database populated by conventional means, that is, physical experiments, does not require many more points than this. For a rolling airframe, such as the FM-3, approximately 600 roll-averaged data points are sufficient for a parameter space that includes Mach number, angle of attack, command level, and roll rate.

Summary

A generic missile has been defined and analyzed to demonstrate the advantages and limitations of an overset grid approach to the aerodynamic performance prediction of rolling airframe missile systems. A computational investigation has been carried out to determine the resolution required for accurate prediction of surface loads, to determine the relative aerodynamic significance of viscous effects, and to validate the model against experimental results. The aerodynamic performance of the missile as a function of angle of attack and canard pitching sequence has also been considered.

A viscous grid system of 8 million points is a good compromise between solution accuracy and case throughput. Instantaneous and roll-average forces and moments from the medium resolution viscous grid are comparable to those obtained in the high resolution baseline solution. Acceptable grid convergence of all forces and moments was obtained.

Significant viscous effects are apparent for the rolling airframe missile system considered. An inviscid solution has no capacity to account for interactions between the canard vortices and the missile boundary layer. The consequence of this inadequacy is incorrect positioning and strength of the inboard canard vortices and incorrect prediction of the secondary effects of the canards on fuselage and fin surface pressures. The inviscid results match well with the viscous solutions when the canards are in transition between maximum positive and negative deflection angles. During this interval, the canard vortices are of minimal strength and the inviscid flow approximation is good.

Computed results agree well with experimental results. Computations of aerodynamic performance as function of angle of attack and the strength of a pitch-up maneuver shows that the increase of control authority beyond 200% command level is limited.

An overset structured grid domain decomposition method enables accurate and efficient simulation of rolling airframe missile

configurations that involve relative motion between system components. Case throughput rates are sufficient to contemplate aerodynamic database population with Navier–Stokes solutions. Note that time-accurate simulation for one rolling airframe case with OVERFLOW-D is much less expensive than generating the same data via corresponding quasi-static solutions for needed roll angles and canard pitch positions.

Acknowledgments

This work was performed under NASA Contract NAS2-00062 to Eloquent. This work was also supported in part by a grant of computer time from the Department of Defense High Performance Computing Modernization Program at the Army Research Laboratory Major Shared Resource Center. The authors gratefully acknowledge the contributions of Michael Aftosmis (NASA) and Scott Murman (Eloquent Corp.) of NASA Ames Research Center. They provided help in converting the FM3 missile geometry definition into a useful format, provided simulation results, and participated in many helpful and interesting discussions. Eric Blades of the Computational Simulation and Design Center of Mississippi State University provided simulation results for comparison. The analytic canard dither model was developed by John Stalnaker of SY Coleman. The expert consultation and assistance provided by Mark Potsdam of the U.S. Army Aeroflightdynamics Directorate at NASA Ames Research Center is also gratefully acknowledged.

References

¹Steger, J., Dougherty, C., and Benek, J., “A Chimera Grid Scheme,” *Advances in Grid Generation*, Vol. ASME FED-Vol 5, American Society of Mechanical Engineers, Fairfield, NJ, 1983.

²Nygaard, T. A., and Meakin, R. L., “An Aerodynamic Analysis of a Spinning Missile with Dithering Canards,” AIAA Paper 2002-2799, June 2002.

³Hall, L. H., “Rolling Airframe Missile Aerodynamic Predictions Using a Chimera Approach for Dithering Canards,” AIAA Paper 2002-0405, Jan. 2002.

⁴Murman, S. M., Aftosmis, M. J., and Berger, M. J., “Numerical Simulation of Rolling Airframes Using a Multilevel Cartesian Method,” *Journal of Spacecraft and Rockets*, Vol. 41, No. 3, 2004, pp. 426–435; also AIAA Paper 2002-2798, June 2000.

⁵Blades, E. L., and Marcum, D. L., “Numerical Simulation of a Spinning Missile with Dithering Canards Using Unstructured Grids,” *Journal of Spacecraft and Rockets*, Vol. 41, No. 2, 2004, pp. 248–256.

⁶Hyams, D. G., Sreenivas, K., Sheng, C., Briley, W. R., Marcum, D. L., and Whitfield, D. L., “An Investigation of Parallel Implicit Solution Algorithms for Incompressible Flows on Multielement Unstructured Topologies,” AIAA Paper 2000-0271, Jan. 2000.


⁷Meakin, R. L., “Automatic Off-Body Grid Generation for Domains of Arbitrary Size,” AIAA Paper 2001-2536, June 2001.

⁸Meakin, R. L., “Adaptive Spatial Partitioning and Refinement for Over-set Structured Grids,” *Computational Methods in Applied Mechanical Engineering*, Vol. 189, 2000, pp. 1077–1117.

⁹Buning, P. G., Jespersen, D. C., Pulliam, T. H., Chan, W. M., Slotnik, J. P., Krist, S. E., and Renze, K. J., “OVERFLOW User’s Manual,” Ver. 1.8, NASA Langley Research Center, Hampton, VA, Nov. 2000.

¹⁰“Defensive Missile Wind Tunnel Test for the Validation and Verification of CFD Codes,” Dynetics, TR PO 40725, Huntsville, AL, Jan. 2002.

P. Weinacht
Associate Editor



Introduction to Aircraft Flight Mechanics: Performance, Static Stability, Dynamic Stability, and Classical Feedback Control

Thomas R. Yechout
U.S. Air Force Academy

With:
Steven L. Morris
David E. Bossert
Wayne F. Hallgren
U.S. Air Force Academy

This textbook is based on a successful 15-year approach to teaching aircraft flight mechanics at the U.S. Air Force Academy.

Intended for junior-level students presented with the material for the first time, the book clearly explains all the concepts and derivations of equations for aircraft flight mechanics. The material progresses through aircraft performance, static stability, aircraft dynamic stability, and feedback control. The chapters present real world applications and contain problems. A solutions manual is available from the publisher.

Contents:

A Review of Basic Aerodynamics • A Review of Basic Propulsion • Aircraft Performance • Aircraft Equations of Motion • Aircraft Static Stability • Linearizing the Equations of Motion • Aircraft Dynamic Stability • Classical Feedback Control • Aircraft Stability/Control Augmentation • Special Topics • Appendices

AIAA Education Series
2003, 628 pages, Hardback
ISBN: 1-56347-577-4
List Price: \$116.95
AIAA Member Price: \$79.95



American Institute of
Aeronautics and Astronautics

Publications Customer Service, P.O. Box 960
Herndon, VA 20172-0960
Phone: 800/682-2422; 703/661-1595 • Fax: 703/661-1501
E-mail: warehouse@aiaa.org • Web: www.aiaa.org